JOURNAL OF GEOPHYSICAL RESEARCH, VOL. 114, A00C21, doi:10.1029/2008JA013547, 2009

Toward adapted time-dependent magnetospheric models: A simple approach based on tuning the standard model

M. Kubyshkina,[1] V. Sergeev,[1] N. Tsyganenko,[1] V. Angelopoulos,[2] A. Runov,[2] H. Singer,[3] K. H. Glassmeier,[4] H. U. Auster,[4] and W. Baumjohann[5]

Received 27 June 2008; revised 11 January 2009; accepted 17 February 2009; published 28 April 2009.

[1] We suggest and test a simple procedure to adapt a magnetic field model by fitting it to observations made simultaneously by several spacecraft. This is done by varying input parameters of a standard model (T96) to find the best fit to the observed field at each time step. As a result we obtain a time-dependent model which can be used for evaluating the quality of the standard model and of the mapping at any particular time, to navigate in the magnetosphere and reproduce its variable configuration during large-scale dynamical events. This procedure was tested using observations made by five Time History of Events and Macroscale Interactions during Substorms (THEMIS) and other complementary (e.g., GOES) spacecraft during the tail season of THEMIS mission (January–March 2008), for which a simplest version of the adapted model was routinely calculated and has been made publicly available. We also use the proton isotropic boundaries observed by low-altitude NOAA spacecraft for independent evaluation of the obtained field models. We found that in quiet conditions deviations of ionospheric footprints between standard and adapted models are generally small (within 1° of latitude), whereas during substorms they may be as large as several degrees, because of stretching and dipolarizations of magnetospheric configuration. We found that the variable tilt of the tail current sheet, partly caused by variations of nonradial component of the solar wind flow, is an additional important factor influencing the modeling result and the mapping quality. By analyzing the adapted models constructed at the time of auroral breakup onset, we conclude that this simple approach is not yet sufficiently accurate to evaluate the source distance in the magnetotail.

Citation: Kubyshkina, M., V. Sergeev, N. Tsyganenko, V. Angelopoulos, A. Runov, H. Singer, K. H. Glassmeier, H. U. Auster, and W. Baumjohann (2009), Toward adapted time-dependent magnetospheric models: A simple approach based on tuning the standard model, *J. Geophys. Res.*, *114*, A00C21, doi:10.1029/2008JA013547.

1. Introduction

[2] The geomagnetic field plays a key role and underlies all events and processes in the solar wind-magnetosphere-ionosphere system. It links the interplanetary medium with the upper atmosphere, guides charged particles, channels low-frequency electromagnetic waves, confines the radiation belts, directs electric currents, controls the flow of plasma, and stores huge amounts of energy, intermittently dissipated in the course of magnetospheric disturbances. The geomagnetic field determines the motion and key properties of the space plasma making it possible to relate observations at different locations by mapping them along the field lines. To understand the behavior of the magnetosphere and its response to the incoming solar wind, one needs a reliable quantitative model of the geomagnetic field that could serve as a road map to observed features.

[3] The Earth's magnetosphere is an extremely dynamical object, owing its exposure to a highly variable and spatially structured solar wind, resulting in intermittent energy buildup and violent dissipation that develop in the magnetotail during substorms. The intrinsic variability of the magnetosphere creates a number of difficulties and limitations in its data-based modeling. A widely used set of products in that area are the empirical models T96, T01, TS04 [*Tsyganenko*, 1995, 2002a, 2002b; *Tsyganenko and Sitnov*, 2005]. In that approach, the model field is constructed using hundreds of thousands of average B vectors, measured in the magnetosphere over a wide range of locations and under different external conditions. The models use different mathematical forms to represent principal magnetospheric field sources, treated as empirically defined functions of the solar wind and IMF parameters. Three shortcomings of these models are known.

[4] First, owing to their statistical nature, they represent some average states, whereas instantaneous field configurations may considerably deviate from the average ones, these

[1]Institute of Physics, Saint Petersburg State University, Saint Petersburg, Russia.
[2]Institute of Geophysics and Planetary Physics, University of California, Los Angeles, California, USA.
[3]Space Weather Prediction Center, NOAA, Boulder, Colorado, USA.
[4]Institut für Geophysik und Extraterrestrische Physik, Technischen Universität Braunschweig, Braunschweig, Germany.
[5]Space Research Institute, Austrian Academy of Sciences, Graz, Austria.

0148-0227/09/2008JA013547$09.00

deviations increase during active periods [*Pulkkinen and Tsyganenko*, 1996] and are, typically, more interesting and important than the average states (e.g., a stressed configuration with embedded thin current sheet that develops prior to the substorm onset). Second, parameterizing the models by the solar wind state may be ambiguous in situations with a variable and inhomogeneous solar wind, because the propagated data from a remote solar wind monitor may be quite inaccurate because of well-known difficulties in calculating the time lags. Third, the accuracy of the model field cannot be easily checked, just because of the lack of a reliable testing method. In the present study we explore one way to avoid these problems, by using an adaptive modeling technique, whose essence is to fit a model to the instantaneous actual magnetospheric field observed by a fleet of magnetospheric spacecraft at some particular time. Our goal is to monitor the magnetosphere continuously, and provide a more accurate mapping along the magnetic field lines. A comparison to predictions of standard models in terms of mapping will then allow to evaluate the mapping quality of the standard models.

[5] The main difficulty to such an approach is the scarcity of observation points (spacecraft) and, hence, incomplete and/or uneven coverage of the modeling region. A few attempts were made previously to realize this idea in rare cases with all available spacecraft located in the near tail region [e.g., *Pulkkinen et al.*, 1991, 2006; *Kubyshkina et al.*, 1999, 2002]. Those studies used the mathematical framework of the above standard models and treated some of their many parameters as variables, with values determined by minimizing the model's standard deviation from the observed field. A major difficulty of that approach was the small number (no more than 4–5) and uneven distribution of spacecraft in the nightside magnetosphere. Insufficient amount of magnetometer data can be partly offset by indirect data, such as the location of the isotropic boundaries, plasma pressure, etc. [e.g., *Kubyshkina et al.*, 2002]. Because of scarcity of favorable events, neither systematic usage nor investigation of that approach was possible in the past studies.

[6] The launch of the Time History of Events and Macroscale Interactions during Substorms (THEMIS) project [*Angelopoulos*, 2008; *Auster et al.*, 2008] opened new possibilities in this area. The mission included a fleet of 5 magnetospheric spacecraft, with the goal to identify the substorm onset mechanism. Their apogees span a wide region between the distances 10 and 30 R_E. Complemented by geosynchronous observations, the spacecraft regularly provide a good coverage of most important tail current systems. This opens a unique possibility to further develop and test our adaptive modeling technique, to explore its capabilities to reveal dynamic changes of the magnetospheric configuration during substorms and convection events. The accuracy of magnetic mapping between the ionosphere and distant magnetosphere is important for resolving the question of where the substorm arc maps in space and for validating the results of THEMIS related to substorm time and substorm trigger location.

[7] In this first paper we describe a simple method to construct a dynamical adaptive model (which has already been routinely run during the entire tail season of THEMIS) and explore its performance using a couple of events during major conjunctions of THEMIS spacecraft. Statistical evaluation of the mapping quality and a more detailed study of substorm onsets and dynamics will be discussed in separate papers.

2. A Simple Approach to the Adaptive Modeling

[8] In this section we concentrate on a simplest possible approach, which can be realized without much intervention of the expert and, therefore, can be routinely applied in the data analysis. The major goal of the next section will then be to reveal the advantages, drawbacks and applicability domain of this approach based on the analysis of a few THEMIS events.

[9] The widely used standard empirical Tsyganenko models (T89, T96, T01, TS04) are flexible enough to represent a wide variety of magnetic field configurations, give a good average representation of observations, and can be completely defined by setting a few input parameters. They are made of blocks describing different magnetospheric current systems (tail, ring, partial ring, and field-aligned currents) each of which is characterized by a relatively large number of linear and nonlinear parameters. Treating all those internal parameters as variables (as was done in some past adaptive models [*Kubyshkina et al.*, 1999, 2002, 2008]), is limited by a few factors. First, in case of adaptive models we always have only a small amount of data, and the number of unfixed variables in any case must not exceed the number of the spacecraft. Second, large number of variables is impractical, as long as we find the solutions at many time steps. Third, the internal parameters are not independent; for example, the tail current systematically shifts earthward with an increase of its intensity, etc. Finally, the main difficulty is that the model field configurations may easily develop nonphysical artifacts like big magnetic islands [*Sergeev et al.*, 2007],which would require a sophisticated case-by-case validation of the modeling results.

2.1. Model Version AM-01

[10] To automate the adaptive modeling, instead of varying the internal parameters one may try to formally treat the external input parameters of the model as "blind" variables, whose values have no relation to the actual solar wind or geomagnetic activity parameters (as it would be the case when using the model in a standard way), but are determined by fitting the model to the data at each time step.

[11] Here we want to underline, that a configuration obtained as a result of this work by no means will be the "best" possible configuration and it does not as well correspond to the "real" magnetic field configuration, which is much more complicated than our representation. We speak about the "best fit" only in the sense of solving a given inverse problem and minimizing the given error function in a given local time sector.

[12] As we believe, during a substorm (or any other activation) there appear transient and spatially limited current structures, which are not included into the basic T96 model. The configuration and time evolution of these currents are not well studied and thus the procedure of including them to the basic model is unclear. Our purpose was to find a possible fit to observations (from T96 class of the models with all possible SW parameters), which is better than T96 with prevailing SW conditions. The differences between the standard model (with observed SW parameters) and the one

obtained here may be thus interpreted as temporal changes of the current systems during an activation in a given (!) MLT sector.

[13] The T89 model has only one (Kp) parameter and is not sufficiently flexible, while the T02 model is limited to only the near tail region ($X > -15\ R_E$). In this study we chose the T96 [*Tsyganenko*, 1995, 1996] as the baseline model. It has four external parameters: the SW dynamic pressure (Pd), hourly averaged *Dst* index, IMF By, and Bz; in the following, we rename these four parameters as PAR1, PAR2, PAR3 and PAR4, respectively, to emphasize their lack of relation to the actual interplanetary and ground-based parameters. At each time step, we compared the magnetic field (Boi) observed at *i*th-spacecraft, located at the position Ri (i = 1,..,N), with the model prediction (Bmi) for the same location with a selected set of input parameters. The fit quality was estimated as:

$$B_{Err} = \frac{1}{WT} \cdot \sum_{i=1}^{N} W_i \cdot \sqrt{\left((B_{OXi} - B_{MX_i})^2 + (B_{OY_i} - B_{MY_i})^2 + (B_{OZ_i} - B_{MZ_i})^2\right)}, \quad (1)$$

where W_i are the weight factors different for each spacecraft, and the total weight $WT = \sum_i W_i$ indicates the number of spacecraft included in modeling. Usage of weighting factors helps to control the spacecraft coverage. In the version discussed below normally $W_i = 1$; otherwise $W_i = 0$ if the *i*th spacecraft was earthward of 5 R_E, or it was outside the magnetosphere. If the distance between two (or more) spacecraft was less than 3 R_E both of them were also assigned a smaller (0.75) weight. The best fit values of the four model parameters were searched using a simple consecutive descent method inside the predetermined limits: [0.1; 10] for PAR1, [−80.; 20] for PAR2, and [−10.;10] for both PAR3 and PAR4. Thus obtained adapted model is referred below as AM-01 model, while the model field calculated by using the actually observed interplanetary parameters and *Dst* is referred to as T96sw. The computation results for both models, for the whole THEMIS tail season (January–March 2008), are publicly available at http://geo.phys.spbu.ru/themis/MODELS_PUBLIC.

2.2. Model Version AM-02

[14] There are a few modifications of this adaptive model algorithm, differing from each other by the inclusion of additional free parameters as well as by inclusion of additional data. In this paper we also present the results of the modification called AM-02, which includes as a new variable the asymptotic tilt of the magnetotail current sheet in the XZ plane of GSM coordinate system. Physically it can be caused either by nonradial solar wind flow, or by some wavy (e.g., flapping) motion of the current sheet, which changes the spacecraft distance from the neutral sheet (and hence the magnetic field produced by the current sheet) and thus affects the mapping results. The variability of the solar wind direction, even though a well-known phenomenon [e.g., *Tsyganenko and Fairfield*, 2004], is rarely taken into account in practical computations, performed almost exclusively in the standard GSM coordinate system. As shown below, this effect is among the principal factors that strongly affects the success of the adaptive modeling. More specifically, irregular variations of the solar wind direction (in particular, Vz variations) change the orientation of the solar-wind-aligned axis of the coordinate system and, hence, change the effective dipole tilt in that system, which results in additional deformation of the neutral sheet surface, as demonstrated in a simulation study by *Sergeev et al.* [2008], which revealed a complicated dynamics and significant amplitude of these deformations. These effects can be taken into account by replacing the standard GSM coordinates by the SW-aligned GSW system [see *Hones et al.*, 1986] and using an appropriately modified value of the dipole tilt angle in the model calculations. A recently released new version of the FORTRAN modeling package (Geopack-2008) includes subroutines for the corresponding coordinate transformations, taking into account the variable solar wind direction; the package is available from http://geo.phys.spbu.ru/~tsyganenko/modeling.html.

[15] When testing the algorithm with this additional free parameter we noticed that the error function (1) often becomes more structured or obeys a less pronounced major minimum, so that sometimes the very different parameter sets produce very similar magnetic fields at the observation points. In the case if all spacecraft were on the same side from the neutral sheet (e.g., below the neutral sheet) in the outer plasma sheet, as typically occurred during January–March 2008 in THEMIS project, a similar increase of the field at a spacecraft often result from physically different effects: either from a growth of the tail current, or from its transverse shift, or from its thinning. In such a case, additional measures are required to stabilize the solution. First, we have limited the range of possible tilt angles within 5° from the maximal observed solar wind tilt (t_0) at that time, obtained as: $t_0 = atan(V_{z_s}w/V_{x_s}w)$, where $V_{x_s}w$ and $V_{z_s}w$ are solar wind velocity components, averaged in 5 min time windows and time shifted to subsolar point. Second, as detailed below, we included additional data, namely, the plasma pressure at two outermost spacecraft, if they were located tailward of $X = -12\ R_E$.

[16] As previously described by *Kubyshkina et al.* [2002], using one-dimensional vertical pressure balance equation in the tail allows us to compute the equivalent lobe field (B_L) above the current sheet at the spacecraft location (x, y) as $B_L(x, y) = \sqrt{\left[2\mu_0 P + \left(B_x^2 + B_y^2 + B_z^2\right)\right]}$, where P and Bx, y, z are the plasma pressure and magnetic field components measured by the spacecraft in the midtail plasma sheet or lobe. The equivalent lobe field B_{L_m} can also be computed in the model at a point (x, y) located 5 R_E northward (or southward) from the neutral sheet. Correspondingly, their difference ($|B_L - B_{L_m}|$) can be easily added to the error function (1). Since the lobe field value is directly related to integral current density in the neutral sheet at the given (x, y) point, this helps to distinguish between the growth of integral current density (total current) and the shift of the neutral sheet or its thinning, as possible causes of the magnetic field changes. In addition, the magnetic field measured by additional spacecraft available at the time of interest in the nearby local time sector (most often GOES spacecraft, Geotail, etc) can be included at this stage. This version of the adapted model is referred to below as AM-02 model.

Table 1. Different Levels of Adaptive Models

Version	Input Data	Parameters Varied	Purposes
AM-01	magnetic field observations on THEMIS only	PAR1-PAR4	routine calculations
AM-02	version 01 input data + magnetic field observations from other spacecraft available in the nearby local time sector + plasma pressure for distant THEMIS (and Geotail if available)	PAR1,PAR2,PAR4,+ additional rotation of a neutral sheet from Sun-Earth radial direction	major conjunction periods
AM-03	version 02 input data + plasma pressure + isotropic boundaries	PAR1,PAR2,PAR3+ additional rotation + addition of a thin current sheet + independent change of the intensity of external current systems	only selected events

2.3. Model Version AM-03

[17] Besides intensifying and displacing the preexisting current sheets, the substorm process may result in the formation of a thin current sheet. Including that feature into the model and, moreover, resolving it with existing spacecraft (which rarely bracket the neutral sheet from both sides) is quite difficult. In any case, such a modification is hard to make without analyzing the obtained configuration at every step by an expert,so it can hardly be automated, and will not be further discussed in this paper.

[18] There are two more additional data sources for the modeling. The first source is the pressure measurements, which can be checked against the pressure values computed from the model under assumption of pressure equilibrium in the plasma sheet as given by

$$\nabla P = \frac{1}{c}[\mathbf{j} \times \mathbf{B}] = \frac{1}{4\pi}[[\nabla \times \mathbf{B}] \times \mathbf{B}], \qquad (2)$$

(for details see *Kubyshkina et al.* [2002]). This option (AM-03, see Table 1) requires large computational resources and will be explored in subsequent papers.

[19] The second source of information is the location of isotropic boundaries of proton and/or electron precipitation measured by low-altitude spacecraft like polar NOAA, DMSP, or FAST. Locations of the isotropic boundary according to the model can be computed using the approximate condition $R_c/r_L \sim 8$ (minimal magnetic field curvature radius divided by the maximal particle gyroradius in the neutral sheet), corresponding to the breakdown of particle adiabaticity (see *Sergeev and Tsyganenko* [1982] and *Kubyshkina et al.* [1999] for more details). We will use that method in the following section as an independent source of information, to compare predictions of different models.

[20] Depending on observations used and input parameters varied we may have several levels of adaptive models, see Table 1.

3. Examples of Application of the Adaptive Modeling

[21] To test the above described procedures we modeled a number of active periods in February–March 2008 with favorable radial large-scale coverage by the THEMIS spacecraft, the so-called major conjunctions. For this presentation we selected two events actively studied by the THEMIS community, which illustrate two different types of dynamical events, the substorms and continuous intense disturbances. In this paper we use magnetic field measurements (from FGM instrument) as well as the total plasma pressure computed by combining the data from two instruments, the electrostatic analyzer covering the plasma below 30 keV (ESA instrument) and the solid state instrument (SST) covering the plasma of higher energies. The instruments are described in detail in the special issue "The THEMIS MISSION" in *Space Science Reviews, 141,* 2008. The adapted models have been constructed with 5 min time step.

3.1. Two Small Substorms on 26 February 2008

[22] Two consecutive substorms developed on the quiet background on 26 February 2008, when the probes were aligned nearly radially along the tail (Figure 1). This events, with substorms having AL amplitudes of ~100 nT and ~200 nT and starting at ~0400 UT and ~0451 UT, respectively, constitute one of most important THEMIS conjunction

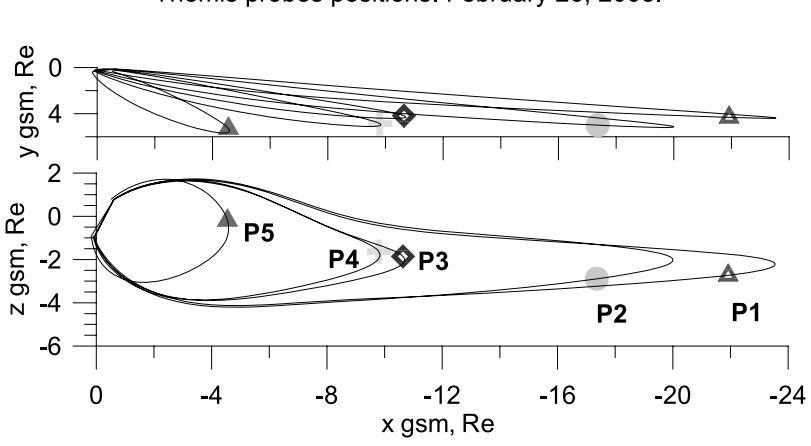

Figure 1. THEMIS probe locations with corresponding T96sw field lines.

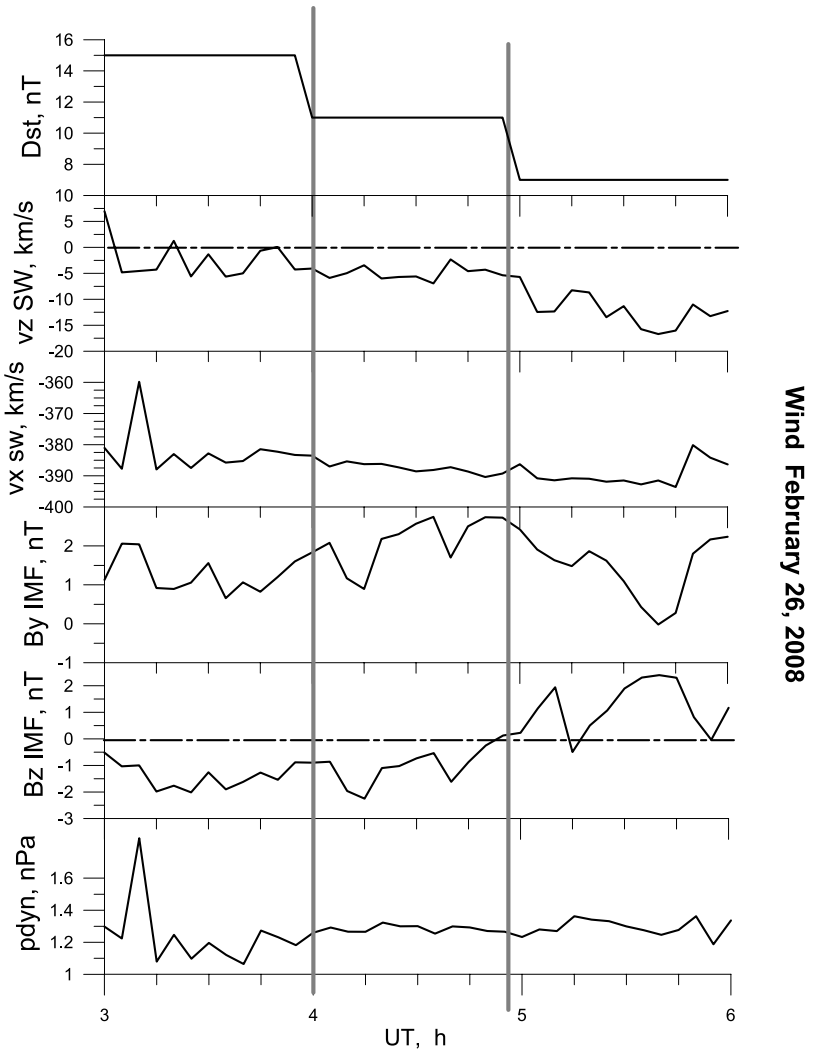

Figure 2. Time-shifted to 10 R_E Wind data (substorm onsets are shown by grey vertical lines).

events, in which the location of the substorm onset in the plasma sheet could be successfully determined.

[23] The corresponding solar wind and *Dst* data for this event are shown in Figure 2. Besides a good spacecraft coverage and good ground observations, this event is all the more favorable because complementary NOAA spacecraft observations of isotropic boundaries in the near-midnight local time sector were also available at that time.

[24] The external part of the observed Bx and Bz magnetic field components (hereafter with the IGRF contribution subtracted) are given in Figure 3 together with the model predictions of solar wind-based T96sw model (blue lines, based on time-shifted solar wind data) and of two adapted models. The lobe field (Figure 3, top) is shown only for the outermost P1 and P2 spacecraft. It was used in the AM-02 model together with GOES 12 spacecraft data (magnetic midnight at 0500 UT) to constrain the model with the current sheet tilt as a free parameter.

[25] One can see that, unlike the standard T96sw model, the AM-01 and AM-02 models reproduce better the observed substorm-scale variations, which include the stretching of the magnetic field lines (enhancement of Bx amplitude) and dipolarization (Bz increase). The smaller amplitudes of the dipolarizations compared to the observations at P3 and P4 spacecraft are not surprising since neither the standard nor the adapted models include the substorm current wedge system, associated with the dipolarizations. We also see that substorm-time magnetic field variations are very different at different meridians: the observed Bx variation looks quite similar at P2 and P3, because of their proximity in local time, though the variation amplitudes are different because of different radial distances, and both are well reproduced by the models AM-01 and AM-02. At the same time, the model yields a similar Bx variation at P4 (located slightly duskward from P3) and at GOES, while observations show a less pronounced Bx variation at that probe. This result indicates that the substorm-related changes of the magnetic field and current are localized in longitude during the substorm expansion phase.

[26] However, there exist important differences between the results of two adapted models. Before the substorm onset the observed lobe field is larger than its quiet level, predicted by the standard model on both P1 and P2. After the substorm onsets at both P1 and P2 probes, it displays small variations associated with intense reconnection and complicated plasma sheet dynamics in that region. By contrast, after 0410 UT the

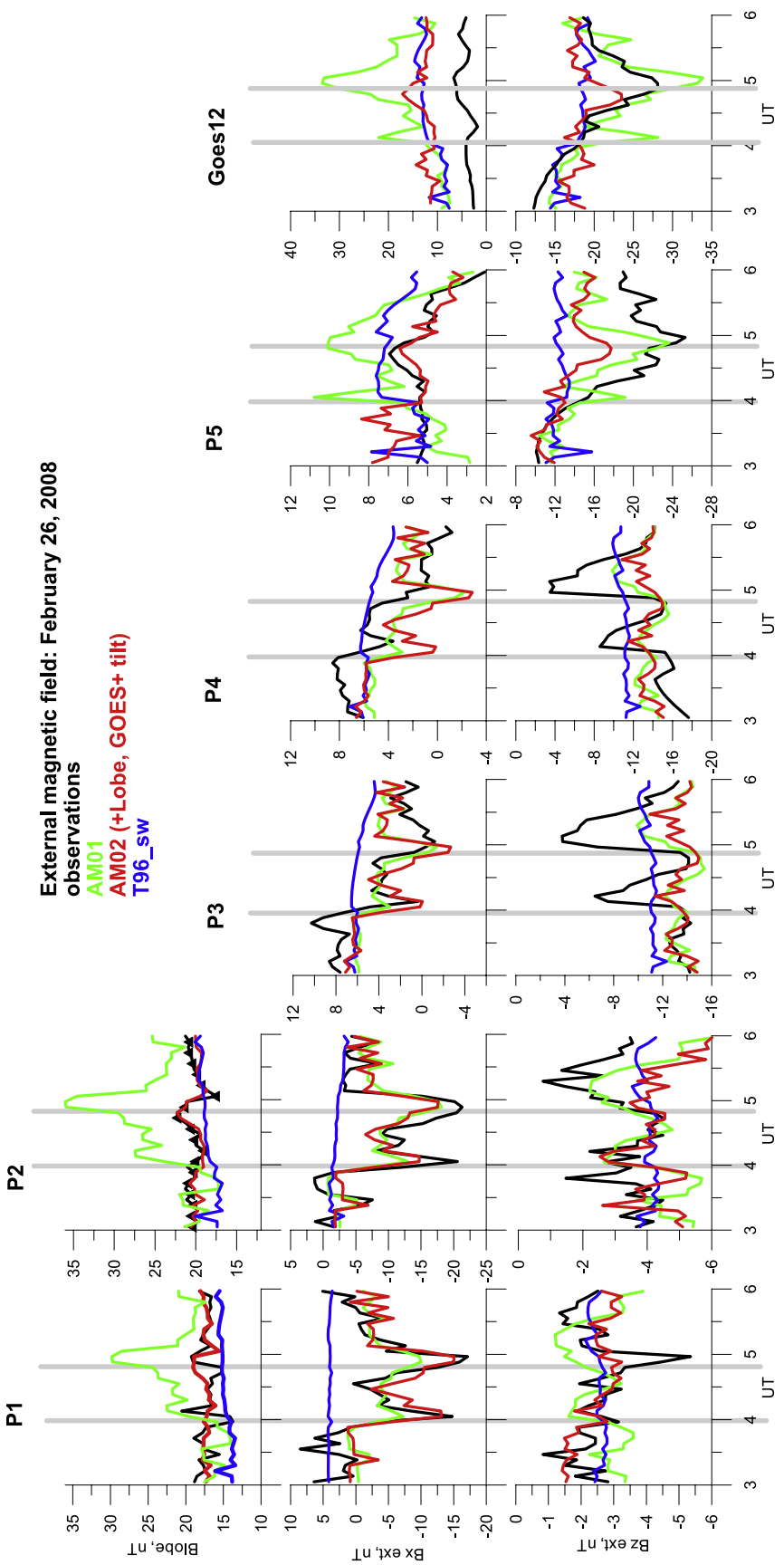

Figure 3. The external part of the observed Bx and Bz magnetic field components (black lines) together with the predictions of standard T96sw model (blue lines) and AM-01 (green line) and AM-02 (red line) models. Vertical light grey lines show the substorms onset times.

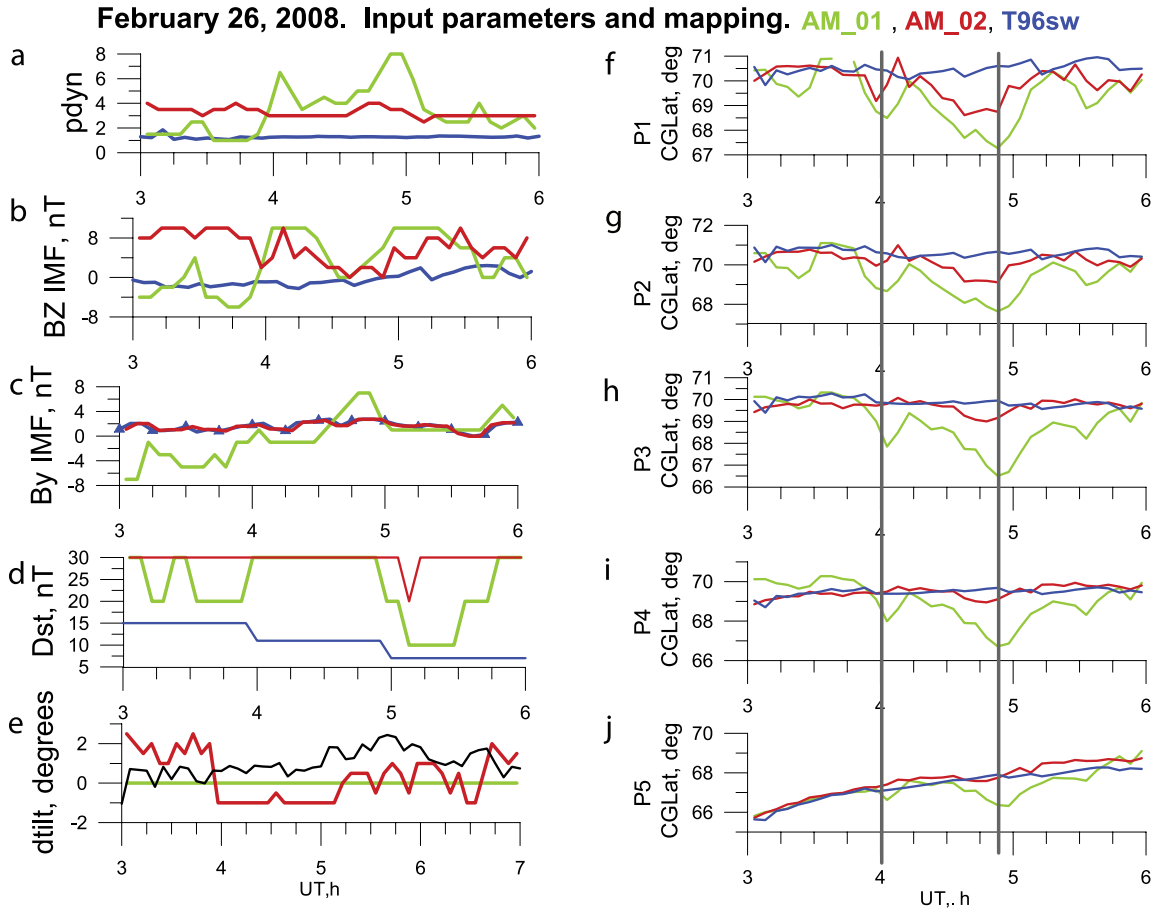

Figure 4. (a–e) Model input parameters together with time-shifted solar wind parameters, *Dst*, and additional tilt of the tail (determined from solar wind velocity as $atan(V_z/V_x)$ in case of observations). Blue lines show the observed solar wind parameters and *Dst* (used for T96), and the parameters of adaptive models are shown by the green lines (AM-01) and by the red lines (AM-02). Observed SW flow tilt in the *xz* plane is given by the black line. (f–j) Corrected geomagnetic latitudes of the ionospheric foot points of THEMIS spacecraft.

AM-01 model (with fixed neutral sheet location) interprets the variations in terms of the enhanced tail current and predicts large lobe field changes, which are not really observed. These artifacts disappear in the AM-02 model which includes the lobe field term in the error function (1). Bx variations are well reproduced by that model in terms of changing the current sheet location (tilt) and other factors. The observed sharp variations of Bx include the change of its sign, demonstrating that the current sheet experienced violent vertical motions during that period, and indicating that at times it also might become rather thin.

[27] Compared to the standard T96 model, the adapted models have much more variable current systems and produce strong variations of magnetosphere-ionosphere mapping. Analyzing Figure 4 we may emphasize the following points:

[28] 1. The spacecraft foot points according to the T96 model shift to highest poleward latitudes, with exception of short periods following the substorm dipolarization after 0400 UT and 0455 UT when the AM-02 model indicated the poleward expansion.

[29] 2. The adapted models indicate the equatorward motion of the foot points before the substorm onset and poleward motion after the onset, which is best seen on distant probes P1 and P2. Amplitude of variations is, however, notably larger in AM-01 version.

[30] 3. Large equatorward shift in ionospheric THEMIS projections before 0500 UT in the AM-01 model is partly nonrealistic, it is probably explained by the overestimated tail current as discussed above.

[31] 4. The behavior of input parameters for the models AM-01 and AM-02 in Figures 4a–4e shows that the intensification of tail current is mostly due to the increase of PAR1 (equivalent to the solar wind dynamic pressure), which is in agreement with previous observational studies by *Wing and Sibeck* [1997] and *Rufenach et al.* [1992]. We note that in our case the IMF By for AM-02 was removed from the set of free parameters and, instead, was taken from observations, on the basis of the fact that it did not significantly affect the results for AM-01. Several previous works [*Cowley*, 1981; *Wing et al.*, 1995] have found notable effects of IMF By in the field line configuration due to magnetospheric tail twist, but the present study cannot consider these effects because we base our modeling on the error function, which is determined by magnetic field components in a given points (spacecraft locations), in which possible tail twisting is less pronounced.

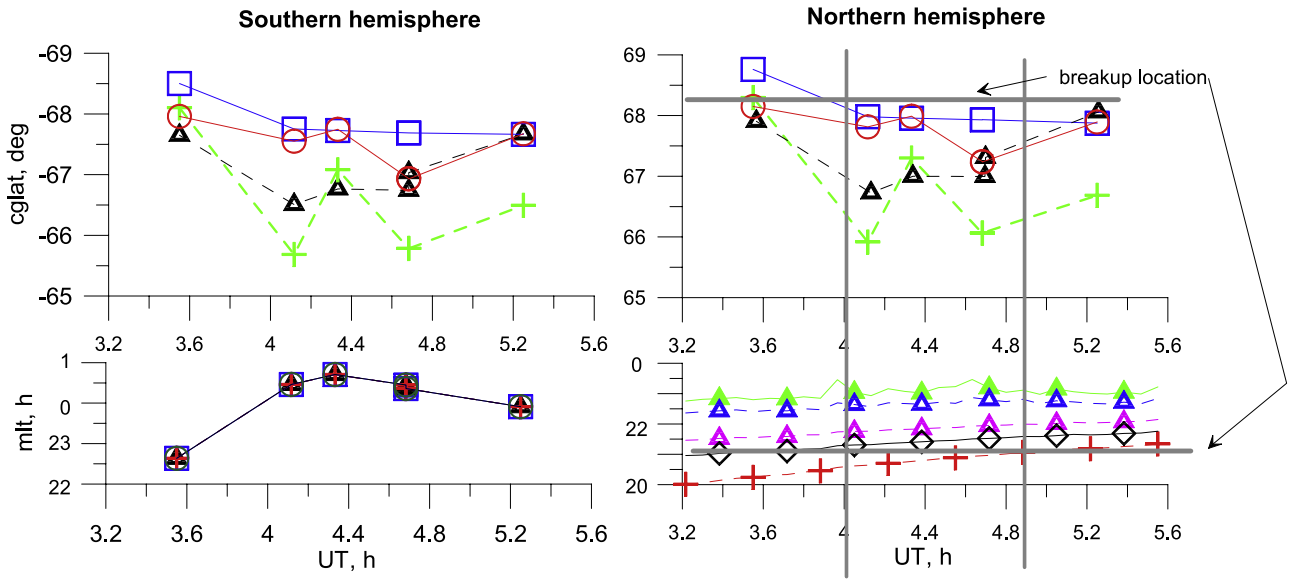

Figure 5. (top left) Corrected geomagnetic latitudes and (bottom left) magnetic local times of proton (>30 keV) isotropic boundaries observed by NOAA in the Southern Hemisphere on 26 February 2008. The observed boundaries are given by black triangles. The model positions of isotropic boundaries are shown by blue squares for T96, by green crosses for AM-01, and by red crosses for AM-02. (top right) Corrected geomagnetic latitudes of the same boundaries mapped along the model field lines into the Northern Hemisphere and (bottom right) magnetic local times of the ionospheric projections of THEMIS probes (from top (green) to bottom (red): P1, P2, P3, P4, and P5).

Thus, for AM-02 model we use the same IMF By as for the basic T96 model, and the differences in mapping due to additional tail twist may be found only in AM-01 version, for which we may have different input parameter (PAR3) instead of observed IMF By.

[32] 5. The variable tilt of the current sheet in Figure 4e seems to be in accordance with the real solar wind flow direction (dtilt = atan(Vz/Vx)) except for sharp upward shift of the neutral sheet between 0400 and 0500 UT.

[33] The spacecraft footprints obtained from different models may differ up to 3–4° of latitude from each other. Which positions are closer to the reality? To find some answer to this question we analyzed the observations of Isotropic boundaries (IB) made by polar NOAA 15, 16 and 17 spacecraft which passed over the nightside auroral zone in the Southern Hemisphere. By identifying the isotropic boundaries in the usual way, as the equatorwardmost location where precipitated and trapped particle flux become nearly equal, we also identified the location of theoretical isotropic boundary in the neutral sheet, conjugate to the NOAA spacecraft trajectory. Fortunately, there were five suitable crossings of NOAA spacecraft near the midnight with well-defined isotropic boundaries of 30 keV protons, presented in Figure 5.

[34] During the time around the first substorm the observed isotropic boundaries (IBs) demonstrate the expected behavior [*Sergeev et al.*, 1993], they are shifted equatorward before the expansion onset and return back after the substorm onset, the same behavior is replicated by the IBs obtained from adapted models. For the second substorm we see no notable additional equatorial motion of the observed IB, which may be explained by either of two factors: (1) the position of the boundary was already shifted from the quiet level (the second activation was initiated more likely by the thin current sheet growth than by the overall enhancement of the tail current) and (2) the boundary observation was made long (20 min) before the second breakup.

[35] The modeled IBs are generally consistent with observed IBs, but they do not coincide and the differences remind us of the lobe field differences found previously in Figure 3. The IB according to the standard T96 model lies poleward of the observed IBs, they nearly agree at the starting and ending points, that is for quiet time periods. The AM-01 model is closer to observations for the first activation and recovery, but it overestimates the stretching for the second activation. The AM-02 model underestimates the first substorm, but gives a correct answer for the second substorm. In this case the models AM-01 and AM-02 give us a corridor where the observations are embedded.

[36] For the second substorm we know the auroral breakup location from the ground optical observations in the Northern Hemisphere [*Angelopoulos et al.*, 2008], which is at (59.3, 263.6) in geographic coordinates, or 68.35° of corrected geomagnetic latitude and 21.55 h of the local time (for corrected geomagnetic coordinates see *Hakura* [1965]). Comparing the mapping curves on Figure 6 (showing the correspondence between the distances in the neutral sheet in the magnetosphere with the CGM latitudes of their ionospheric foot points) we see a large difference in the predictions of the source distance. The T96 and AM-02 models suggest that the breakup latitude is mapped into the dipole-like region well within 10 R_E. All THEMIS spacecraft in these models (T96, AM-01) map to higher latitudes than the auroral breakup location (see blue and red crosses, marking probes projections). This disagrees with determination of the activation region in the magnetosphere [*Angelopoulos et al.*,

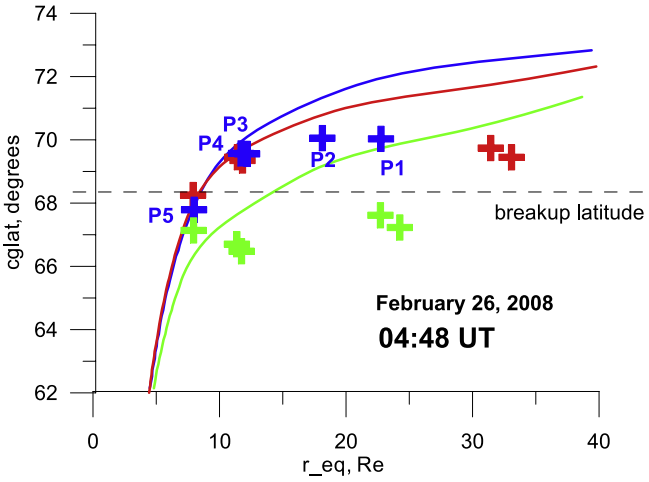

Figure 6. Mapping curves for Gillam meridian (263.6° of geographical latitude) for different models: T96 (blue), AM-01 (green), and AM-02 (red). The estimated corrected geomagnetic latitude of the auroral breakup is shown by the dashed black line. Colored crosses mark the projections of THEMIS probes, obtained with corresponding models.

2008] according to which the most probable activation distance was at around 20 R_E. On the contrary, the AM-01 model gives the auroral breakup distance of ~13 R_E with P1, P2 probes located at higher latitude, and P3, P4 probes at lower latitude as compared to that of the auroral breakup. This is more consistent with magnetospheric source determination results but, as we already know, this model gives too large lobe field and hence cannot be trusted. This conflict shows that the models T96sw, AM-01 and AM-02 probably do not represent realistic magnetospheric-ionospheric mapping because the current sheet thickness variation is not yet included into the model.

3.2. Substorm and Enhanced Convection During the Major Conjunction on 5 March 2008

[37] Another period of major conjunction of THEMIS spacecraft is 5 March 2008, which includes an isolated substorm onset that commenced at ~0604 UT, then was followed by ~10-h-long active period (AL up to 500 nT), and was concluded by a strong ~1000 nT substorm after 1400 UT. For our purposes, it is also an interesting event, demonstrating the important role of nonradial solar wind flows in the adaptive modeling. Also, many isotropic boundary observations are available on the nightside during this event. THEMIS configuration for this period is given in Figure 7, and *Dst* and solar wind parameters are shown in Figure 8.

[38] The 5 March 2008 event was very favorable for the analyses from the solar wind viewpoint, because the phase front normals available from OMNI Web site did not deviate much from the Sun-Earth line, also the solar wind velocity was rather stable (405 ± 5 km/s) which facilitates the time-shifting procedure. Moreover, by shifting Wind data by 49 min to the bow shock nose position, we got an excellent agreement of this time shifted IMF variations with those observed by the Geotail, which was located closely to the bow shock nose at that time (not shown here). Figure 8b shows a large positive Vz component of the solar wind above 20 km/s during a long period between 0400 and 1400 UT, which may cause a northward shift of the magnetotail current

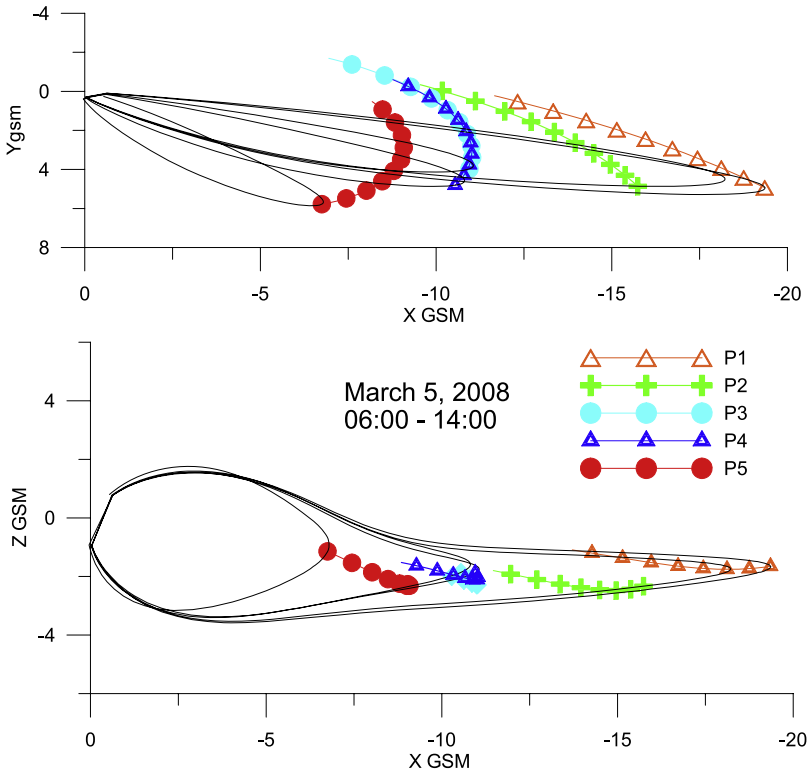

Figure 7. THEMIS configuration for the period 0600–1400 UT, 5 March 2008, and magnetic field lines for the beginning of the interval, i.e., for 0600 UT.

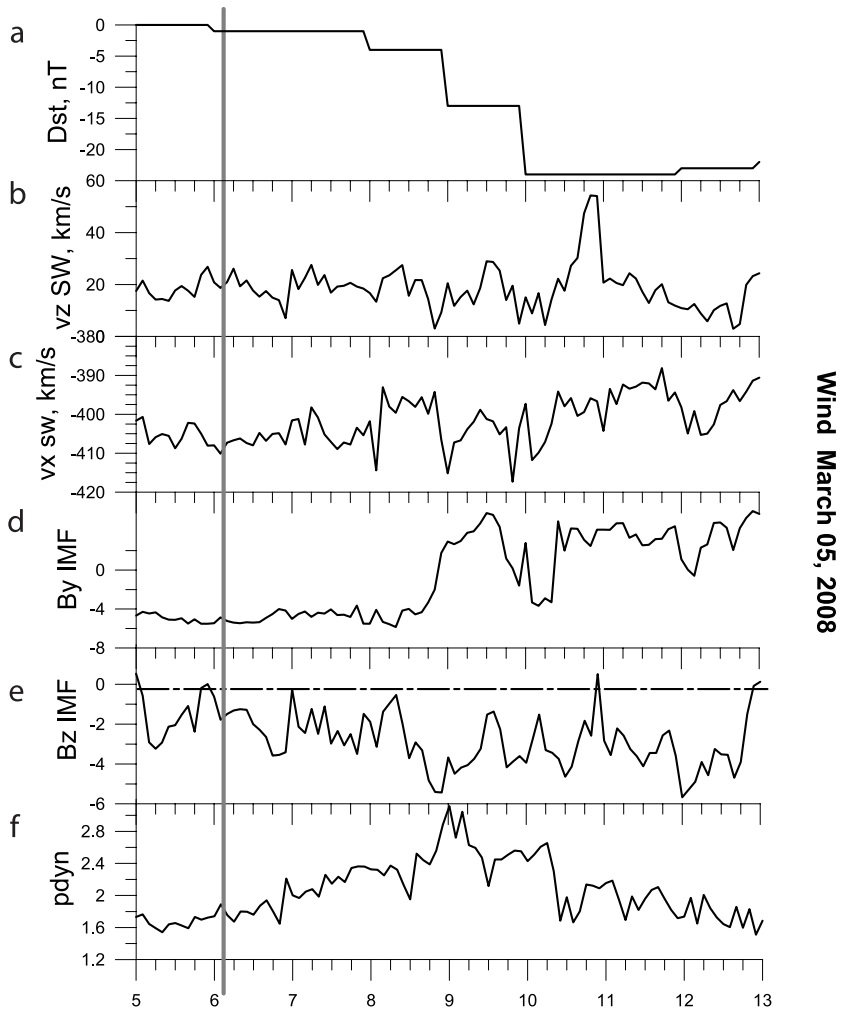

Figure 8. *Dst* and solar wind parameters for 5 March 2008. (a) Equatorial *Dst* values from WDC for Geomagnetism, Kyoto; (b and c) *z* and *x* components of solar wind velocity in GSM coordinates; (d and e) *y* and *z* components of interplanetary magnetic field; and (f) solar wind dynamic pressure.

sheet (Vz $\sim$ 20 km/s corresponds to 3° tilt for Vx = 400 km/s). In the other solar wind parameters we do not see anything unusual: the values of Vx and Pd are stable and close to the norm, a comparably large By, and negative fluctuating Bz are observed during almost the entire period of ground activity between 0500 and 1500 UT.

[39] The observed and modeled magnetic field components (presented in the same way as in Figure 3) are given in Figure 9.

[40] Comparing observations with the predictions of standard T96sw, we see a large (more than 10 nT) depression in the Bx component, it is observed at all spacecraft including GOES. The substorm-like dipolarization in Bz component is seen at all spacecraft after 0615 UT. The standard model gives a good representation for Bz component on P3 and P4 probes (at $\sim$11 R_E equatorial distance), while it overestimates negative perturbation in Bz at the distant probes P1 and P2 (15 and 20 R_E) and underestimates it at the near-Earth P5 and GOES 11 spacecraft. The Blobe value is also underestimated by T96, but the difference in Bx component between observations and standard model is less than 5 nT(10 nT) for the P1 (P2) probe. Unfortunately we had plasma data from P2 probe only at the beginning of the interval, so that only data from the P1 probe were used to construct the AM-02 model after 0730 UT.

[41] A large systematic discrepancy in the Bx component between T96 and observations seen at all spacecraft may be related to either (1) global increase of the tail current or (2) northward shift of the neutral sheet. The difference between the current density profiles along the neutral sheet and the neutral sheet locations in different models is illustrated in Figure 10 for 0605 UT epoch, at the end of the substorm growth phase. The AM-01 model is designed to use only the first option, and its results demonstrate the greatly increased peak current strength, which causes a large discrepancy in the lobe field. In the AM-02 model, which may use either option, the total current remains enhanced, but to a smaller degree, and the matching of Bx component is basically produced by the northward shift of the neutral sheet from its standard position. This shift can be as large as 0.5 R_E at r = 10 R_E and exceeds 1.5 R_E at r = 18 R_E in Figure 10, which are very large values, comparable to the characteristic thickness of the current sheet.

[42] In spite of the good overall agreement of AM-02 predictions to observations, from Figure 9 one may see that Bz component of the magnetic field is better reproduced by

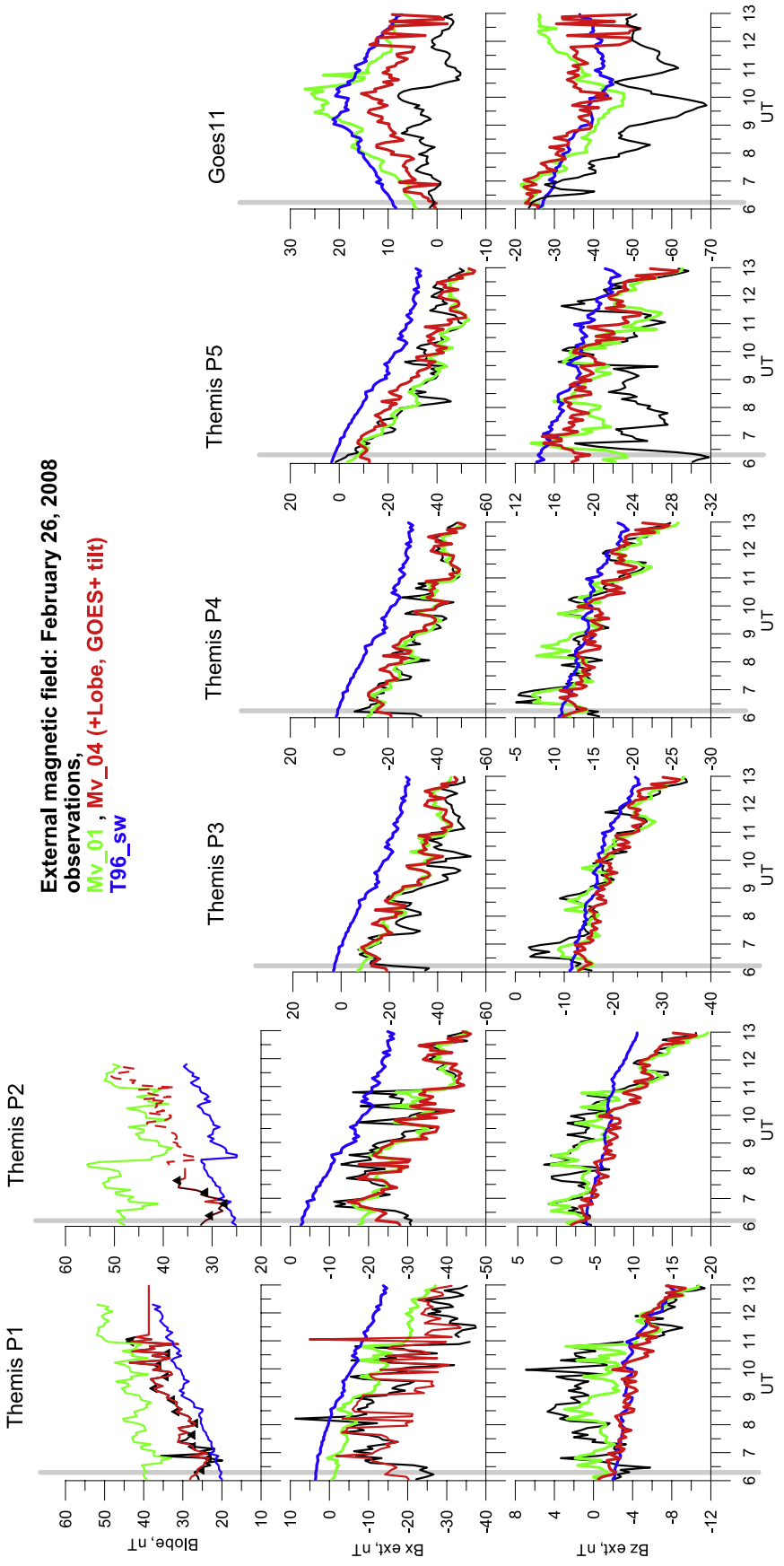

Figure 9. The same as in Figure 3 but for the 5 March 2008 event.

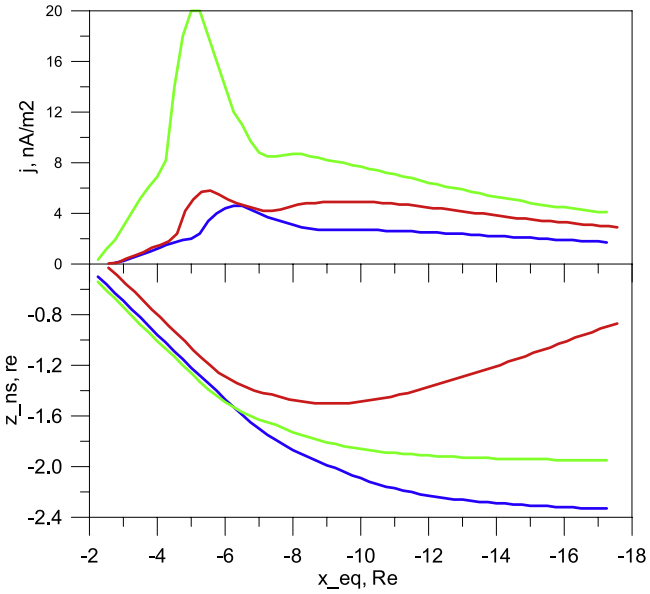

Figure 10. (top) Profiles of current density in the neutral sheet along the magnetospheric tail at 0605 UT 5 March 2008 and (bottom) the position of neutral sheet center calculated from different models: T96sw (blue), AM-01 (green), and AM-02 (red).

the AM-01 model compared to AM-02. This means that the configuration provided by the AM-02 model, is still significantly different from the actual one.

[43] By inspecting the ionospheric mapping results and model parameters presented in Figure 11, we verify the conclusions made by studying the 26 February event. T96sw model again limits the polewardmost locations of the foot points, whereas AM-01 provides their equatorward limit (which can be as different as 5–6° below the T96sw predictions). One can also notice that AM-02 model sometimes gives spacecraft projections about 0.5° poleward from T96 value in the period between 0900 and 1200 UT. An interesting fact is that, though the field lines in the AM-02 model are more stretched than in T96 so that the models are very different (see Figure 10), the spacecraft projections appear to be quite close to T96 values in the northern auroral zone (with reasonable deviations during activations up to ±1.0° in geomagnetic latitude), being offset by the neutral sheet displacement.

[44] From the behavior of the model parameters (Figures 11a–11e) we again see that the increase of currents in both models AM-01 and AM-02 is due to the increased value of PAR1 (Pdyn), while the other parameters are closer to the observed ones. We again see that the additional current sheet tilt in the AM-02 model generally follows the behavior of the solar wind flow direction, though it includes some more variations. We suppose that these variations are partly unreal and appear because of the similar effects of the current increase and of the neutral sheet transverse motion with

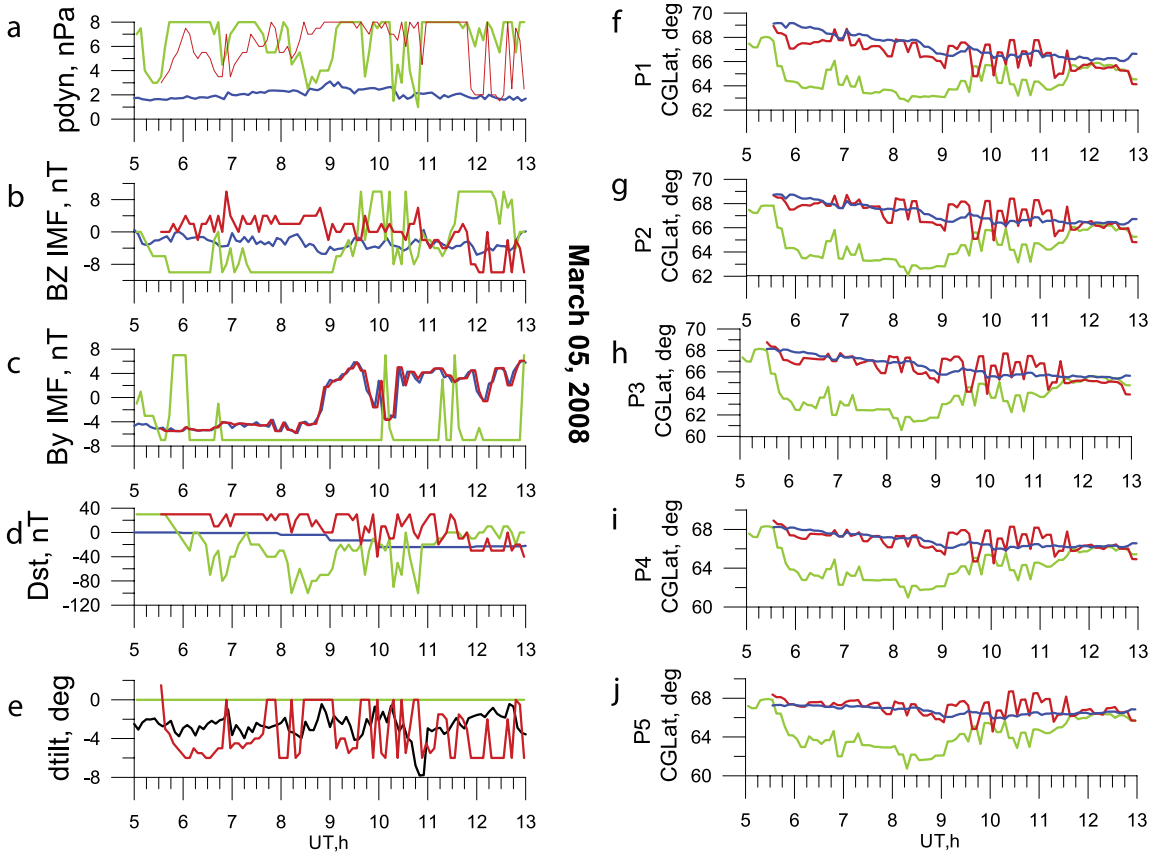

Figure 11. The same as in Figure 4 but for 5 March 2008 event.

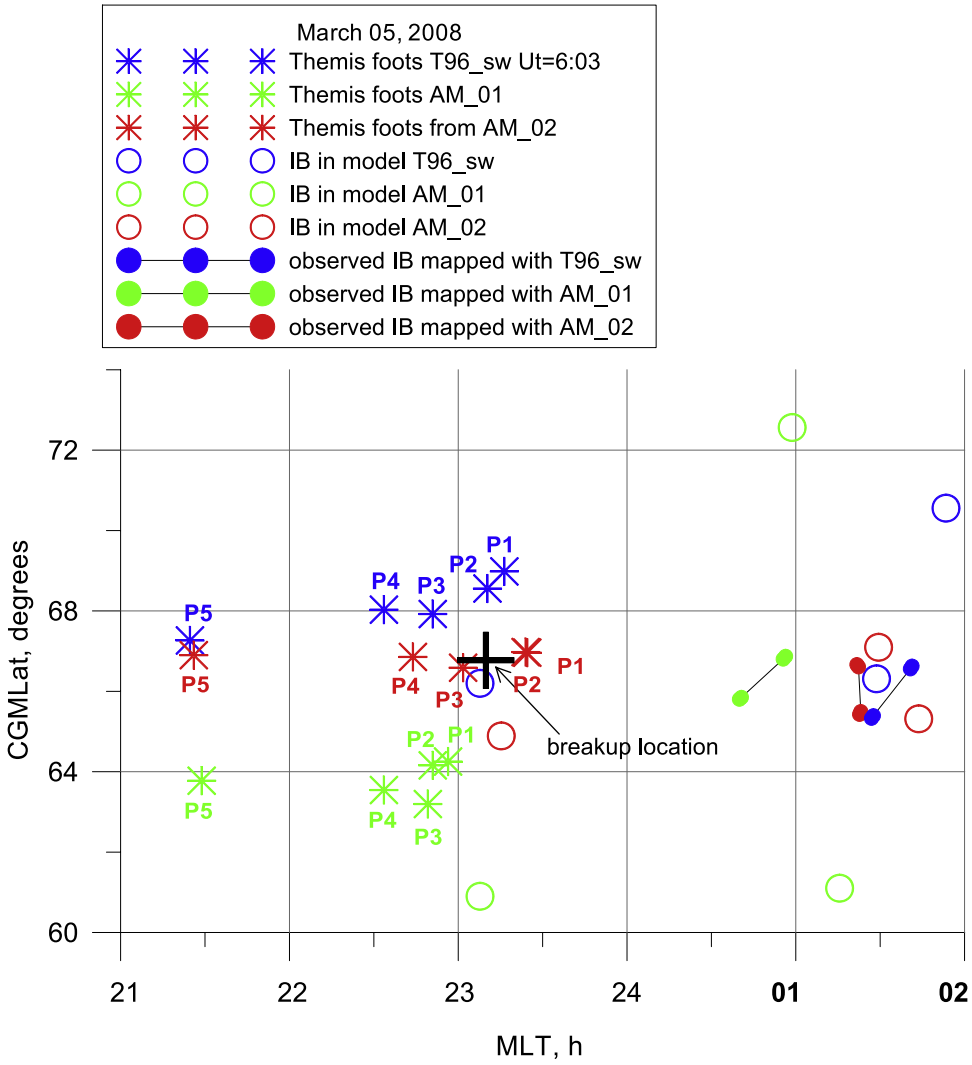

Figure 12. Isotropic boundaries and spacecraft foot points at 0605 UT, 5 March 2008. The solid circles show the positions of the observed boundaries mapped to the Northern Hemisphere using a corresponding model: T96 (blue), AM-01 (green), and AM-02 (red). Open circles in the 0100–0200 MLT sector with corresponding color give the model predictions for the corresponding (proton and electron) boundaries. Open circles near 2300 MLT show the model prediction for the proton (>30 keV) IB position at the onset meridian, and the colored stars mark the ionospheric foot points of THEMIS probes.

respect to the spacecraft. Indeed, by comparing the variations of the additional tilt (Figure 11e) with variations of pdyn and IMF Bz between 1200 and 1300 UT, one may see that the increase in the negative angle value corresponds to a decrease in Pdyn and IMF Bz (which results in a decrease of the tail current).

[45] To check the mapping quality for this event we again compare the model predictions of the IB position with those observed by the NOAA spacecraft. Unfortunately, the bulk of observations during that period was made at a different local time, shifted by more than 2.5 h to the dawn side from the local time sector probed by the THEMIS spacecraft, so the quality of the adapted model can degrade toward the meridian of NOAA observations. That is why we present here (see Figure 12) only one set of IB observations made just prior to the substorm onset at ~0603 UT by NOAA 17 spacecraft. We use here the isotropic boundaries of both the protons of >30 keV energy and the electrons of >100 keV energy.

[46] Here we compare not just observed and modeled IB for two species, we compare observed IBs mapped to the Northern Hemisphere with northern IB foot points computed from the model. In fact it has to be a comparison of two pairs of circles: for example of two filled red and two empty red. Figure 12 shows that the best correspondence between the positions of the observed and modeled IBs at ~1.5 h MLT meridian, as well as in the latitudinal difference between electron and proton boundaries, is obtained when using the AM-02 adapted model.

[47] We also plotted on Figure 12 the positions of model IBs, calculated near the meridian of substorm breakup location (opened circles around MLT = 23.2). According to ground optical observations,the 0614 UT substorm breakup was located above Gillam, thus it may be roughly placed at CGMLat = 66.3, MLT = 23.25 h. which is well above the IB position calculated from AM-02 and too close to the IB, calculated from T96sw model.

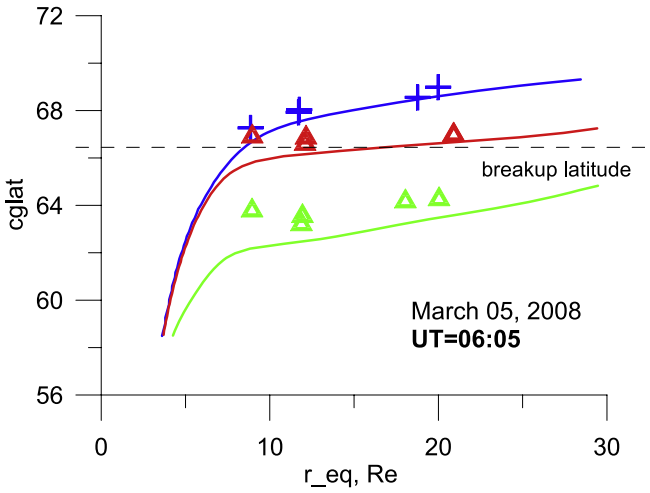

Figure 13. The same as Figure 6 but for 5 March 2008. Mapping curves for Gillam meridian (263.6° of geographical latitude) for different models: T96 (blue), AM-01 (green), and AM-02 (red). The estimated corrected geomagnetic latitude of the auroral breakup is shown by the dashed black line. Colored crosses mark the projections of THEMIS probes, obtained with corresponding models.

[48] From Figure 11 one may see that the difference in latitudes between the T96 and AM-02 models, which we consider as the best approximation available, is within 1°, which is not too much. Still the mapping curves and the near-equatorial magnetic configuration are significantly different. Figure 13 shows the mapping curves for the Gillam meridian. One can see that the breakup position at 66.3 CGMLat is mapped to closer than 10 R_E with T96 and to ~15 R_E with AM-02. Moreover, the mapping curve for the best (AM-02) model is very steep, so that a small change in the breakup latitude results in a large jump of the equatorial distance. Therefore, as in the previous section, we rather conclude that in the current spacecraft configuration and with the simplest adaptive algorithms discussed, the adaptive models alone cannot provide the required accuracy/reliability to identify the position of the breakup source region.

4. Concluding Remarks

[49] We have shown that, even using a very simple algorithm, varying the input parameters of standard magnetospheric models, the tested adaptive methods proved as useful tools for a quick evaluation of the quality of magnetospheric models and their mapping properties. They may be successfully used for large-scale systems of multiple magnetospheric spacecraft, like THEMIS. Here we introduced two first versions of the adaptive models, which are suitable for routine data processing and do not require much computational resources and supervising efforts.

[50] 1. The simplest version of the adaptive models (AM-01) is fast and easy to use for long observation periods; it is recommended to be run in conjunction with the T96 (or other standard) model. The good agreement between the standard and AM-01 model during magnetically quiet times indicates a good mapping quality for such periods. A larger discrepancy for disturbed periods indicates potential problems, yields margins for possible foot point locations, and points out a need to pay more attention to improving the model. Variations of magnetic field components in that version are obtained mostly by overall scaling of the currents intensities, which often leads to the overestimation of total tail current, larger current densities and, hence, excessive equatorial shift of the ionospheric projections of mapped foot points. Thus we conclude that during disturbed periods the AM-01 model rather indicates an equatorial limit for possible spacecraft projection in a given local time sector.

[51] 2. The next version of the adaptive model (AM-02), is also easy to use but that version requires additional data (e.g., the plasma pressure) to control the total tail current. AM-02 version was shown to provide a better approximation to real configurations than the AM-01 and the standard model. Still during periods when a thin current sheet may form in the spacecraft vicinity (increasing the current density, but not the total current and lobe field) the requirement of the pressure balance may result in an underestimate of the field lines stretch near the neutral sheet. Thus the AM-02 version, being the most accurate among three above-discussed models, probably yields a poleward limit for the spacecraft projection in a given local time sector.

[52] AM-02 in most aspects is closer to T96 than to AM-01, though B values on the spacecraft are more similar in AM-01 and AM-02. This may be explained by a very large deviation of Blobe, modeled with AM-01, from observations and other models, which means overestimated current densities, hence overestimated stretching, which may be seen clearly in Figure 10 on the profiles of current density and integral current density shown for all 3 models.

[53] 3. Both THEMIS major conjunction events presented in this work illustrate how important is the variable tilt of the tail current sheet, partly caused by the nonradial component of the solar wind flow. The importance of taking into account the variable tilt was demonstrated in all recent adaptive modeling efforts [e.g., *Sergeev et al.*, 2005, 2007; *Cao et al.*, 2008], in which the modeling was done in a different way: by changing the parameters of the currents inside the model, but also including the variable tilt. Thus the variable tilt is a critical factor, which may significantly change the mapping results: a small tilt can result in a notable change in the ionospheric projections and considerably change the asymmetry between the foot points in the Northern and Southern hemispheres.

[54] 4. The peculiarity of THEMIS configuration during the tail season of 2008 was that during the major conjunctions the spacecraft were southward from the neutral sheet, which makes it difficult to separate the effects of the current sheet tilt and its thinning. Partly because of that difficulty, the constructed models were unable to provide a sufficient accuracy to determine the source location by a simple mapping of the breakup location into the ionosphere along the magnetic field lines of the adapted model. The mapping curves are usually very steep (see, e.g., red curve in Figure 13), and the difference between two extreme types of the models AM-01 and AM-02 is still large. A proper inclusion of the current sheet thinning as well as the inclusion of all available pressure measurements are currently among our top priorities in improving the technique of the adaptive modeling. On the

other hand, the orbits planned for the year 2009 are expected to be closer to the neutral sheet during major conjunctions, which will help us to come up with more accurate modeling results.

[55] **Acknowledgments.** The energetic particles observations on board the polar NOAA spacecraft have been made available by NOAA, and solar wind observations from Wind spacecraft have been made available via CDAWeb and OMNI Web sites. We thank Amanda Prentice for her help in preparing the manuscript. The work was supported by the THEMIS contract NAS5-02099. The work by V.S. and M.K. was also supported by Russian Ministry of Science grants, by the RFBR grants 07-02-91703 and 07-05-91109, and CRDF grant 2861. We thank both referees for fruitful discussion and help in evaluating the manuscript.

[56] Amitava Bhattacharjee thanks David Sibeck and another reviewer for their assistance in evaluating this paper.

References

Angelopoulos, V. (2008), The THEMIS mission, *Space Sci. Rev.*, *141*, 5–34, doi:10.1007/s11214-008-9336-1.

Angelopoulos, V., et al. (2008), Tail reconnection triggering substorm onset, *Science*, *23*, 931–935.

Auster, H. U., et al. (2008), The THEMIS fluxgate magnetometer, *Space Sci. Rev.*, *141*, 235–264, doi:10.1007/s11214-008-9365-9.

Cao, X., et al. (2008), Multispacecraft and ground-based observations of substorm timing and activations: Two case studies, *J. Geophys. Res.*, *113*, A07S25, doi:10.1029/2007JA012761.

Cowley, S. W. H. (1981), Magnetospheric asymmetries associated with the Y-component of the IMF, *Planet. Space Sci.*, *29*, 79–96.

Hakura, Y. (1965), Tables and maps of geomagnetic coordinates corrected by the higher order spherical harmonic terms, *Rep. Ionos. Space Res. Jpn.*, *19*, 121–157.

Hones, E. W., Jr., R. D. Zwickl, T. A. Fritz, and S. J. Bame (1986), Structural and dynamical aspects of the distant magnetotail determined from ISEE-3 plasma measurements, *Planet. Space Sci.*, *34*, 889–901.

Kubyshkina, M. V., V. A. Sergeev, and T. I. Pulkkinen (1999), Hybrid Input Algorithm: An event-oriented magnetospheric model, *J. Geophys. Res.*, *104*(A11), 24,977–24,993.

Kubyshkina, M. V., V. A. Sergeev, S. V. Dubyagin, S. Wing, P. T. Newell, W. Baumjohann, and A. T. Y. Liu (2002), Constructing the magnetospheric model including pressure measurements, *J. Geophys. Res.*, *107*(A6), 1070, doi:10.1029/2001JA900167.

Kubyshkina, M., T. I. Pulkkinen, N. Ganushkina, and N. A. Partamies (2008), Magnetospheric currents during sawtooth events: Event-oriented magnetic field model analysis, *J. Geophys. Res.*, *113*, A08211, doi:10.1029/2007JA012983.

Pulkkinen, T. I., and N. A. Tsyganenko (1996), Testing the accuracy of magnetospheric model field line mapping, *J. Geophys. Res.*, *101*, 27,431–27,442.

Pulkkinen, T. I., D. N. Baker, D. H. Fairfield, R. J. Pellinen, J. S. Murphree, R. D. Elphinstone, R. L. McPherron, J. F. Fennell, R. E. Lopez, and T. Nagai (1991), Modeling the growth phase of a substorm using the Tsyganenko model and multi-spacecraft observations: CDAW-9, *Geophys. Res. Lett.*, *18*(11), 1963–1966.

Pulkkinen, T. I., N. Y. Ganushkina, E. I. Tanskanen, M. Kubyshkina, G. D. Reeves, M. F. Thomsen, C. T. Russell, H. J. Singer, J. A. Slavin, and J. Gjerloev (2006), Magnetospheric current systems during stormtime sawtooth events, *J. Geophys. Res.*, *111*, A11S17, doi:10.1029/2006JA011627.

Rufenach, C. L., R. L. McPherron, and J. Schaper (1992), The quiet geomagnetic field at geosynchronous orbit and its dependence on solar wind dynamic pressure, *J. Geophys. Res.*, *97*(A1), 25–42.

Sergeev, V. A., and N. A. Tsyganenko (1982), Energetic particles losses and trapping boundaries as deduced from calculations with a realistic magnetic field model, *Planet. Space Sci.*, *30*, 999–1007.

Sergeev, V. A., M. Malkov, and K. Mursula (1993), Testing the Isotropic Boundary Algorithm method to evaluate the magnetic field configuration in the tail, *J. Geophys. Res.*, *98*, 7609–7620.

Sergeev, V. A., et al. (2005), Transition from substorm growth to substorm expansion phase as observed with a radial configuration of ISTP and Cluster spacecraft, *Ann.Geophys.*, *23*, 2183–2198.

Sergeev, V., et al. (2007), Observation of repeated intense near-Earth reconnection on closed field lines with Cluster, Double Star and other spacecraft, *Geophys. Res. Lett.*, *34*, L02103, doi:10.1029/2006GL028452.

Sergeev, V. A., N. A. Tsyganenko, and V. Angelopoulos (2008), Dynamical response of the magnetotail to changes of the solar wind direction: An MHD modeling perspective, *Ann. Geophys.*, *26*, 2395–2402.

Tsyganenko, N. A. (1995), Modeling the Earth's magnetospheric magnetic field confined within a realistic magnetopause, *J. Geophys. Res.*, *100*(A4), 5599–5612.

Tsyganenko, N. A. (1996), Effects of the solar wind conditions on the global magnetospheric configuration as deduced from data-based field models, *Eur. Space Agency Spec. Publ.*, *ESA SP-389*, 181–185.

Tsyganenko, N. A. (2002a), A model of the near magnetosphere with a dawn-dusk asymmetry: 1. Mathematical structure, *J. Geophys. Res.*, *107*(A8), 1179, doi:10.1029/2001JA000219.

Tsyganenko, N. A. (2002b), A model of the near magnetosphere with a dawn-dusk asymmetry: 2. Parameterization and fitting to observations, *J. Geophys. Res.*, *107*(A8), 1176, doi:10.1029/2001JA000220.

Tsyganenko, N. A., and D. H. Fairfield (2004), Global shape of the magnetotail current sheet as derived from Geotail and Polar data, *J. Geophys. Res.*, *109*, A03218, doi:10.1029/2003JA010062.

Tsyganenko, N. A., and M. I. Sitnov (2005), Modeling the dynamics of the inner magnetosphere during strong geomagnetic storms, *J. Geophys. Res.*, *110*, A03208, doi:10.1029/2004JA010798.

Wing, S., and D. G. Sibeck (1997), Effects of interplanetary magnetic field Z component and the solar wind dynamic pressure on the geosynchronous magnetic field, *J. Geophys. Res.*, *102*, 7207–7216.

Wing, S., P. Newell, D. Sibeck, and K. Baker (1995), A large statistical study of the entry of interplanetary magnetic field Y-component into the magnetosphere, *Geophys. Res. Lett.*, *22*(16), 2083–2086.

V. Angelopoulos and A. Runov, Institute of Geophysics and Planetary Physics, University of California, Los Angeles, CA 90095, USA.

H. U. Auster and K. H. Glassmeier, Institut für Geophysik und Extraterrestrische Physik, Technischen Universität Braunschweig, Mendelssohnstrasse 3, D-38106 Braunschweig, Germany.

W. Baumjohann, Space Research Institute, Austrian Academy of Sciences, A-8042 Graz, Austria.

M. Kubyshkina, V. Sergeev, and N. Tsyganenko, Institute of Physics, Saint Petersburg State University, 198504 Saint Petersburg, Russia. (kubysh@geo.phys.spbu.ru)

H. Singer, Space Weather Prediction Center, NOAA, Boulder, CO 80305, USA.